Journal of Biomechanics 105 (2020) 109760

Contents lists available at ScienceDirect

Journal of Biomechanics

journal homepage: www.elsevier.com/locate/jbiomech
www.JBiomech.com

Heterogeneous matrix deposition in human tissue engineered cartilage changes the local shear modulus and resistance to local construct buckling

Jill M. Middendorf [a], Caroline Dugopolski [b], Stephen Kennedy [b], Eric Blahut [b], Itai Cohen [c], Lawrence J. Bonassar [a,d,*]

[a] Sibley School of Mechanical Engineering, Cornell University, Ithaca, NY, USA
[b] Histogenics Corporation, Waltham, MA, USA
[c] Physics, Cornell University, Ithaca, NY, USA
[d] Meinig School of Biomedical Engineering Cornell University, Ithaca, NY, USA

ARTICLE INFO

Article history:
Accepted 20 March 2020

Keywords:
Cartilage repair
Microscale mechanics
Buckling
Tissue engineering
Spectroscopy

ABSTRACT

Human tissue engineered cartilage is a promising solution for focal cartilage defects, but these constructs do not have the same local mechanical properties as native tissue. Most clinically relevant engineered cartilage constructs seed human chondrocytes onto a collagen scaffold, which buckles at low loads and strains. This buckling creates local regions of high strain that could cause cell death and damage the engineered tissue. Since human tissue engineered cartilage is commonly grown in-vivo prior to implantation, new matrix deposition could improve the local implant mechanics and prevent local tissue buckling. However, the relationship between local biochemical composition and the local mechanics or local buckling probability has never been quantified. Therefore, this study correlated the local biochemical composition of human tissue engineered cartilage constructs using Fourier transform infrared spectroscopy (FTIR) with the local shear modulus and local buckling probability. The local shear modulus and local buckling probability were obtained using a confocal elastography technique. The local shear modulus increased with increases in local aggrecan content in the interior region (inside the scaffold). A minimum amount of aggrecan was required to prevent local construct buckling at physiologic strains. Since the original scaffold was primarily composed of collagen, increases in collagen content due to new matrix deposition was minimal and had little effect on the mechanical properties. Thus, we concluded that aggrecan deposition inside the scaffold pores is the most effective way to improve the mechanical function and prevent local tissue damage in human tissue engineered cartilage constructs.

1. Introduction

Tissue engineered cartilage has shown the capacity to fill focal cartilage defects with components of native cartilage such as collagen and proteoglycans. However, spatial patterns of biochemical composition are different from native tissue. Additionally, the local modulus of engineered cartilage is typically more compliant than native cartilage (Khoshgoftar et al., 2013). Multiple studies have attempted to recreate the depth dependent modulus of native tissue in engineered cartilage, but have been unsuccessful (Kim et al., 2017; Klein et al., 2007; Luo et al., 2017; Ng et al., 2005; Ph et al., 2003; Poole et al., 2001; Schinagl et al., 1997). In part, it has been difficult to achieve similar mechanical properties to native cartilage, since the relationship between local biochemical composition and local mechanics are unknown.

Currently, the relationship between local biochemical composition and the local mechanical properties of engineered cartilage is believed to be identical to native articular cartilage. In native tissue collagen networks and collagen crosslinks provide resistance to shear deformation (Poole et al., 2001; Stading and Langer, 1999; Wilson et al., 2007; Wu and Herzog, 2002). Additionally, aggrecan, a highly charged molecule, provides resistance to compression (Leroux et al., 2000; Williamson et al., 2001). Although native cartilage provides a good basis to understand engineered cartilage, the lower concentrations and different distributions of collagen and

* Corresponding author at: Department of Biomedical Engineering, 149 Weill Hall, Cornell University, Ithaca, NY 14853, USA.
E-mail address: lb244@cornell.edu (L.J. Bonassar).

https://doi.org/10.1016/j.jbiomech.2020.109760
0021-9290/

aggrecan content may reveal a distinct local structure–function relationship.

These lower concentrations of collagen and aggrecan content in engineered cartilage have only been measured globally. This global relationship shows that increasing both collagen and aggrecan increases the shear modulus (Byers et al., 2008; Cigan et al., 2016; Wan et al., 2011). Additionally, this correlation can vary based on the starting material (collagen, alginate, agarose, etc.) and its structure (scaffold, hydrogel, etc.) (Ng et al., 2005; Steck et al., 2010). Most studies using hydrogels show relatively small increases in both collagen and aggrecan can increase the modulus (Byers et al., 2008; Cigan et al., 2016; Erickson et al., 2009; Klein et al., 2007; Mauck et al., 2002). However, in clinically relevant constructs using collagen membranes or foams (Behrens et al., 2006; Brittberg, 2010; Crawford et al., 2012, 2009; Kon et al., 2013; Nixon et al., 2015), aggrecan not collagen increased the construct modulus (Griffin et al., 2016; Krase et al., 2014; Middendorf et al., 2017a). These global structure function relationships demonstrate that both the scaffold and new matrix deposition affect the modulus, however heterogeneous new matrix deposition creates local tissue weakness that cannot be identified globally.

In clinically relevant tissue engineered cartilage constructs, these local tissue weakness include non-linear phenomenon such as construct buckling (Freyman et al., 2001; Gibson, 2005; Gibson and Ashby, 1997; Harley et al., 2007). Construct buckling may cause local regions of high strain under compression (the buckling onset) and due to joint friction (shear loading). This buckling may cause local tissue damage and cell death due to the high local tissue strain (Bartell et al., 2015). During in-vitro culture prior to implantation (Crawford et al., 2012) new matrix deposition, specifically global aggrecan content, must reach a minimum value to adequately reinforce the scaffold to prevent buckling (Middendorf et al., 2017b). However, global measures of aggrecan content may not fully predict local construct buckling. Determining the relationship between local biochemical composition and local construct buckling could identify a minimum local collagen and aggrecan concentration required to prevent damage via buckling.

Recently, micro-spectroscopy techniques, including Fourier transform infrared spectroscopy (FTIR), have been developed to quantify the local collagen and aggrecan concentration in tissue engineered cartilage (Boskey and Pleshko Camacho, 2007; Kim et al., 2005; Kunstar et al., 2013; Rieppo et al., 2012; Silverberg et al., 2014). In engineered cartilage these quantitative biochemical measurements have successfully identified global mechanical function of engineered cartilage, but not local mechanics (Hanifi et al., 2017; Karchner et al., 2017). However, FTIR has been used to identify the local structure function relationship in native articular cartilage. These recent advances in spectroscopy techniques create the opportunity to correlate local biochemical concentrations with local mechanical properties measured through confocal elastography.

Therefore, the goal of this study was to use FTIR spectroscopy and confocal elastography to quantify the local structure–function relationship of human tissue engineered cartilage. The local biochemical composition will be correlated with the local shear modulus and the local probability of buckling. This analysis will be performed on human tissue engineered cartilage constructs similar to constructs in advanced clinical trials (Crawford et al., 2012, 2009). Specifically, we will examine how new matrix deposition reinforces scaffolds locally to improve the local shear modulus and prevent local buckling. Such microscale mechanisms could be used in conjunction with in situ micro-spectroscopy techniques to predict construct mechanical performance prior to implantation.

2. Methods

2.1. Construct preparation

Constructs were prepared using a modified version of a previously reported technique (Appendix A) (Crawford et al., 2012, 2009). Constructs were removed from culture at 0-, 1-, and 5-weeks post seeding, then frozen at −20 °C. A total of 18 constructs were created with 6 constructs from each time point. Each construct was cut in half. One half was used for depth-dependent shear modulus (Buckley et al., 2010; Middendorf et al., 2017b; Silverberg et al., 2013) and buckling analysis, while local biochemical composition was measured on the other half.

2.2. Depth-dependent mechanics

The local shear modulus of each construct was obtained using a previously established confocal elastography technique (Buckley et al., 2010; Middendorf et al., 2017b; Silverberg et al., 2013). Briefly, hemi-cylinder constructs were exposed to 14 μg/ml 5-dic hlorotriazinyl-aminofluorescein (5-DTAF) (Molecular Probes1, Grand Island, NY) for 30 min followed by a 20 min rinse in phosphate buffer saline (PBS, Corning Cellgro, Manassas, VA). Constructs were mounted between two plates, placed on an inverted Zeiss LSM 510 5 live confocal microscope (Carl Zeiss AG, Oberkochen, Germany), and imaged using a 488 nm laser. Both compression and shear were imaged at a frame rate of 20fps. Buckling was analyzed in constructs that were compressed to 10% axial strain. After reaching equilibrium, constructs were subjected to a 1% oscillatory shear strain at a frequency of 0.5 Hz.

The microscale strain measured under compressive and shear loading was determined using an open source digital image correlation (DIC) (Blaber et al., 2015) software in MATLAB (Mathworks, Natick, MA). This software tracked displacement of grid points (79 μm apart), then calculated strain at each grid point under both compressive and shear loading. Under shear loading, the shear strain was averaged at each depth of the construct. Shear stress was calculated by measuring the force on the sample and dividing by the construct cross-sectional area, which remained constant with depth. Then, the depth-dependent shear modulus was calculated by dividing shear stress amplitude by the depth-dependent shear strain amplitude.

2.3. Buckling analysis

Because these constructs buckle under compression (Middendorf et al., 2017b), we quantified the local buckling probability in 5-week constructs. Local buckling (Figure Supplementary 1A-1B) was determined using a previously established buckling threshold based on the transverse strain (strain orthogonal to loading, Figure Supplementary 1C) (Middendorf et al., 2017b). This technique examines the strain obtained from the DIC code at every grid point. If the transverse strain, Eyy, was greater than the buckling threshold (Eyy > 2%), then that location was considered buckled (Figure Supplementary 1C). This strain threshold was previously determined as the best at identifying the difference between buckled regions (Figure Supplementary 1D). The buckling probability was calculated as the number of buckled points divided by the total points in one column of the DIC grid.

2.4. Fourier transform infrared spectroscopy (FTIR)

To obtain local biochemical composition, FTIR data collection and analysis was performed using a previously established technique (Appendix A) (DiDomenico et al., 2019; Silverberg et al.,

2014). Once FTIR data was obtained and analyzed, relative biochemical concentrations (FTIR fit coefficients) were mapped onto a white light image of the sample to create a visual representation of the collagen and aggrecan concentration. Depth-dependent biochemical concentrations were obtained by averaging the fit coefficients at each tissue depth. During processing of the 0-week and 1-week constructs, compression due to cutting and mounting was noted. To account for this sectioning artifact, all collagen concentrations were normalized to the average for 5-week constructs. All constructs with a periphery region were aligned by registering the interface of the scaffold surface with periphery, then the local biochemical composition was compared to the local shear modulus and buckling probability.

2.5. Histology

To verify the FTIR analysis, 5-week samples were sectioned for histology. Additional 4 μm thick sections were cut from the paraffin-embedded blocks and placed onto glass slides. Safranin-O/Fast green staining was used to visually identify proteoglycan distribution (Rosenberg, 1971). Picrosirius red stain was used to visually identify collagen distribution.

2.6. Statistics

Linear correlations were evaluated between depth-dependent biochemical data and shear modulus for all constructs. A goodness of fit parameter, R^2, was reported for all linear correlations. To determine a local buckling threshold for collagen and aggrecan content, the relationship between local collagen or local aggrecan content, x, was correlated with the local buckling probability, P_B, using a sigmoid function in MATLAB.

$$P_B = b + \frac{a-b}{1+10^{(EC50-x)*d}} \quad (1)$$

where a and b are the maximum and minimum plateau values, respectively. EC50 and d are the inflection point and the slope at the inflection point respectively. The best fit curve was calculated using an orthogonal least square fitting algorithm. To ensure both the buckling probability and biochemical concentration contributed equally to the least squares fit, both variables were standardized. A goodness of fit parameter was reported as the root mean squared error (RMSE) of the standardized variables. Fit coefficients and standardized variables were then transformed back into the raw variables and plotted.

3. Results

3.1. Local biochemical composition

FTIR spectroscopy provided a quantitative measurement of local collagen and aggrecan concentrations. FTIR maps of collagen and aggrecan showed similar patterns to Picrosirius red and Safranin-O staining respectively (Fig. 1). In 0- and 1-week constructs, FTIR maps showed uniform amounts of high collagen concentration and low aggrecan concentration throughout the construct (Figure Supplementary 2). In 5-week constructs both the collagen fit coefficients and the Picrosirius red staining showed the most collagen in the interior region. Aggrecan fit coefficients and Safranin-O staining showed high aggrecan concentrations in the scaffold periphery and lower aggrecan concentration in the interior region. These maps indicate that quantitative coefficients reflect the qualitative staining patterns observed in histology.

These FTIR maps were then plotted to understand how the relative concentrations of collagen and aggrecan change with depth

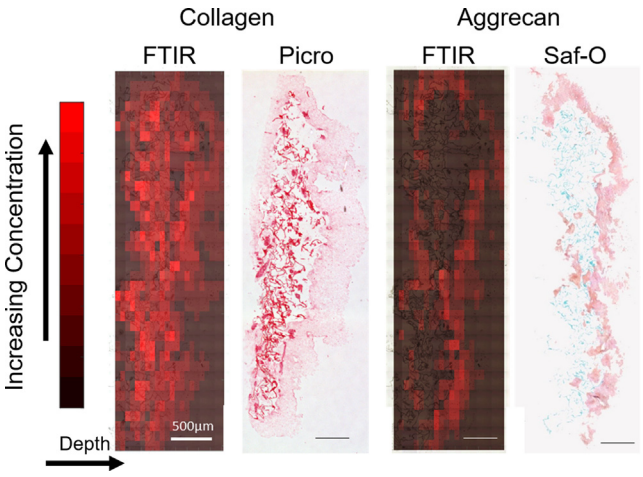

Fig. 1. FTIR spectroscopy provides detailed spatial patterns of both aggrecan and collagen content. These patterns match the patterns found in histology stains for collagen (picrosirius red) and proteoglycans (Safranin-O, scale bar = 500 μm). (For interpretation of the references to colour in this figure legend, the reader is referred to the web version of this article.)

and with respect to the initial scaffold (periphery and interior region). Small changes in collagen content occurred in 0- and 1-week constructs (Fig. 2A). In 5-week constructs collagen content did not change at any depth. Relative aggrecan content depended on where the chondrocytes deposited new matrix. Aggrecan was not present in 0-week constructs, so reported values likely reflect the resolution limit of this technique (Fig. 2B). More aggrecan was present in 1-week constructs than 0-week constructs. Aggrecan content in 5-week constructs was about twice as large as 1-week constructs and about 5 times larger than 0-week constructs. Global measures of biochemical concentration as measured

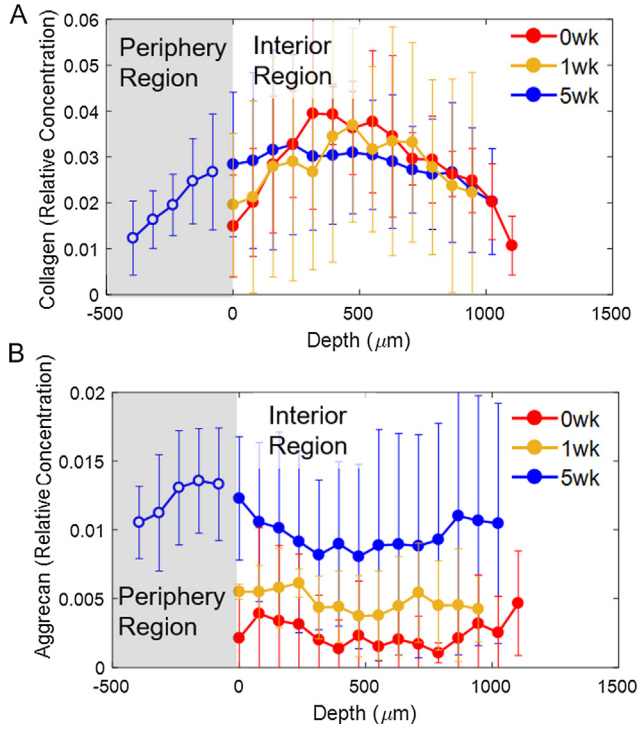

Fig. 2. Quantitative relationship between (A) collagen and (B) aggrecan versus depth for all constructs. The biochemical concentrations change based on region (periphery or interior).

through biochemical assays (dimethylmethylene blue assay, DMMB) (Enobakhare et al., 1996; Puetzer et al., 2013) and (hydroxyproline assay) (Neuman and Logan, 1950) are highly correlated with average fit coefficients obtained from FTIR microscopy (Figure Supplementary 3).

During construct growth, aggrecan content was deposited heterogeneously with preferential deposition in the periphery region. In the interior region, aggrecan concentration varied by multiple orders of magnitude (0.001–0.028) while collagen content varied by a factor of four (0.01–0.039, Fig. 3A). Since the periphery region is characterized by new matrix deposition and no scaffold, only 5-week constructs contained a periphery region. The periphery region showed small changes in collagen and aggrecan content (Fig. 3B) with about 50% more aggrecan and slightly less collagen than the interior region.

3.2. Local shear modulus

Confocal elastography techniques created visual strain maps (Fig. 4), which were used to calculate the local shear moduli. In 0- and 1-week constructs, the shear modulus did not change much with depth. The moduli of 5-week constructs was almost double the moduli of both 0- and 1-week constructs. The periphery region of 5-week constructs had a shear modulus almost half that of the interior region (Fig. 5).

When local biochemical concentration of the interior region was plotted against the local shear modulus, aggrecan concentration had the largest effect on the shear modulus. No trends were observed between the shear modulus and the collagen concentration (R^2 = 0.008, p = 0.98, Fig. 6A). In contrast, increasing aggrecan resulted in an increase in the local shear modulus (R^2 = 0.57, p < 0.001, Fig. 6B). To examine potential interactions between collagen and aggrecan, all data were fit to surface plots (R^2 = 0.61p < 0.001, Figure Supplementary 4). These fits were statistically similar to the linear fits for aggrecan alone, suggesting that the interaction of collagen and aggrecan did not provide any additional predictive power. Aggrecan, not collagen, has the largest effect on the local shear modulus in the interior region.

In contrast, neither collagen nor aggrecan affected the shear modulus of the periphery region. No strong correlations were observed between the interior and periphery regions (R^2 = 0.34, p = 0.30 and R^2 = 0.45, p = 0.22 for collagen and aggrecan respectively, Fig. 6C, D). The differences between the interior and periphery regions indicate the location of matrix deposition relative to the initial scaffold affects the resulting shear modulus.

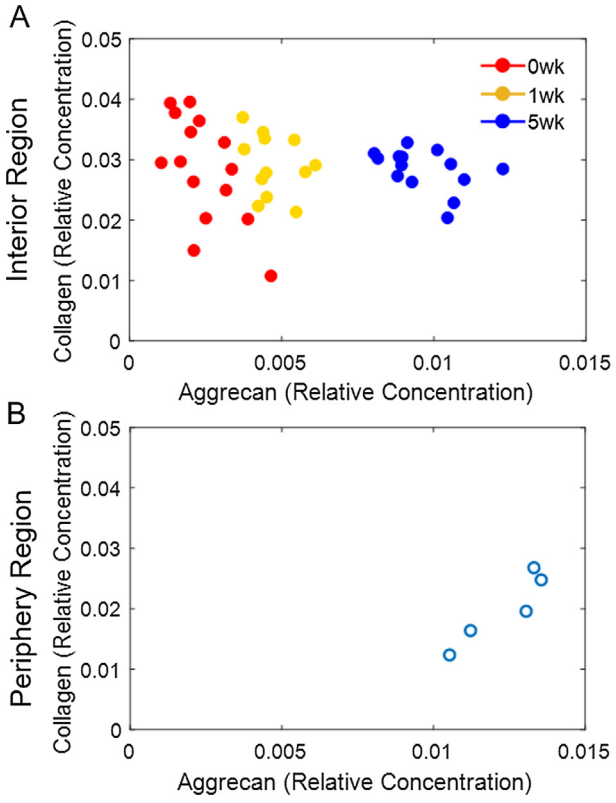

Fig. 3. The span of collagen and aggrecan concentration in the (A) interior region and the (B) periphery region. Biochemical data are the average for a depth at a given time point. Error bars are not shown for clarity and can be found in Fig. 2.

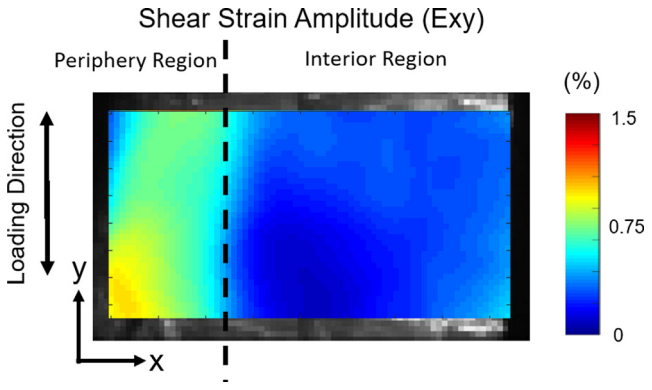

Fig. 4. Local shear strains caused by shear loading in a 5-week construct.

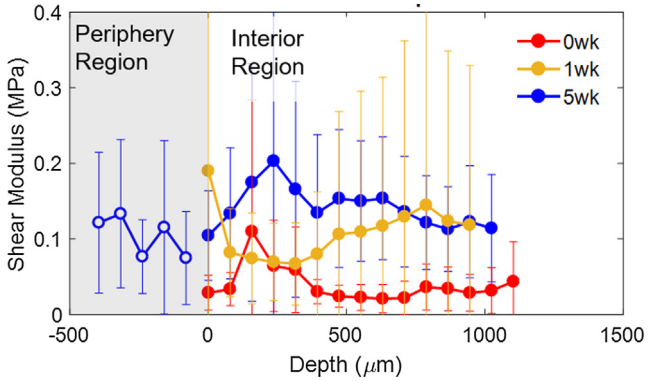

Fig. 5. Quantitative relationship between shear modulus versus depth for all constructs.

3.3. Local construct buckling

A dose–response curve identified that a minimum local aggrecan concentration is required to prevent local scaffold buckling under 10% axial strain in 5-week constructs. Collagen concentration was not a good predictor of buckling (RMSE = 0.99, Fig. 7A), because the range of buckling probabilities at both high and low collagen concentrations was large (0–0.79 and 0.18–0.63 respectively). In contrast, aggrecan is a good predictor of buckling. Low aggrecan concentration resulted in uniformly high buckling probabilities (~75%, 0.56 to 0.79), while high aggrecan concentrations (~0.0060) resulted in a zero-buckling probability (RMSE = 0.40, Fig. 7B). The most reliable predictor of buckling was the fractional aggrecan content ($\frac{Aggrecan}{Aggrecan+Collagen}$), which demonstrated a clear threshold between buckled and non-buckled regions (ratio = 0.19,

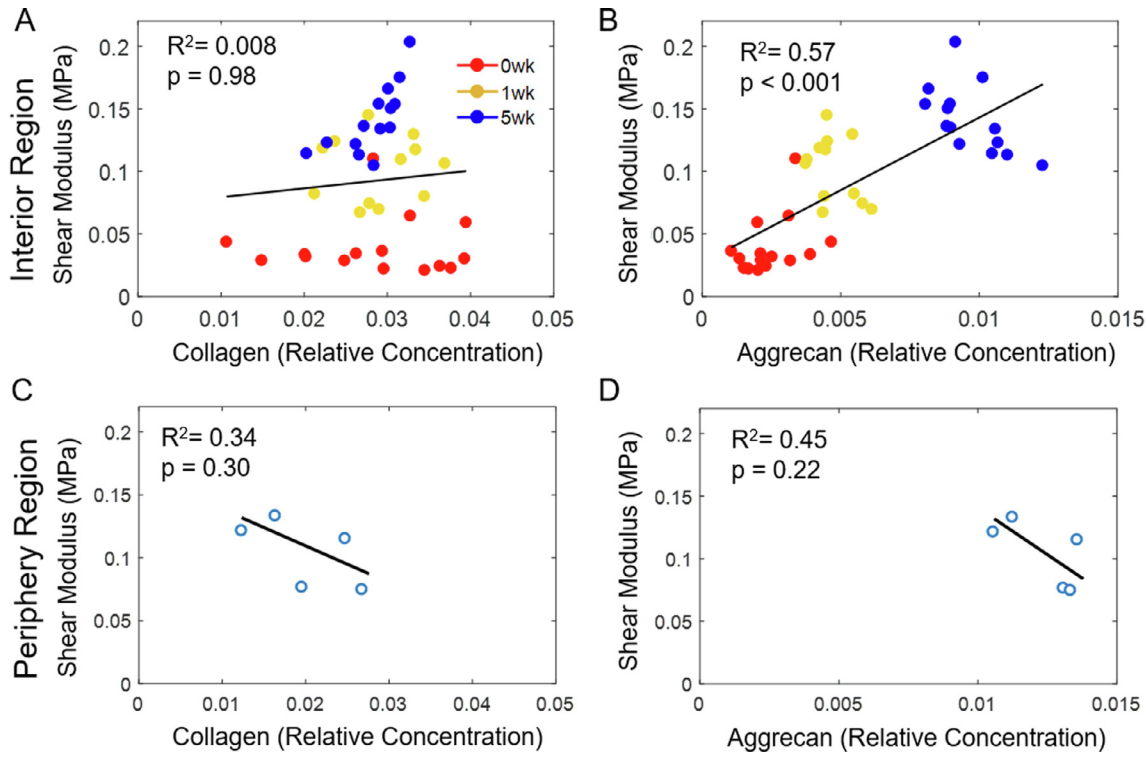

Fig. 6. The relationship of the shear modulus with the relative collagen and aggrecan concentration (A) Collagen concentration in the interior region does not predict the shear modulus (R^2 = 0.35, p = 0.98), (B) Increases of aggrecan content resulted in increases in shear modulus (R^2 = 0.57, p < 0.001, N = 41) (C) The shear modulus in the periphery region is not well predicted by either collagen content (R^2 = 0.34, p = 0.30) or (D) aggrecan content (R^2 = 0.45, p = 0.22). Different correlations were noted between the periphery and the interior regions (N = 5). Biochemical data and shear modulus values are the average for a depth at a given time point. Error bars are not shown for clarity and can be found in Figs. 2 and 5.

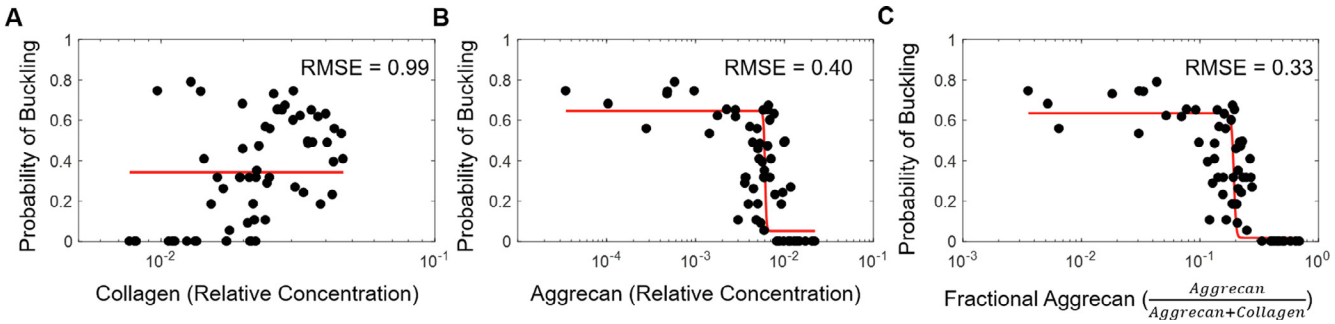

Fig. 7. The relationship between local construct buckling and biochemical content follows a sigmoidal function (A) Collagen concentration does not affect buckling (RMSE = 0.99). (B) The buckled fraction at a given depth stays constant until a threshold of aggrecan is reached at 0.0060, at which point buckling does not occur (RMSE = 0.40). (C) The ratio of aggrecan to collagen content in engineered cartilage constructs reveals a threshold at 0.19 between buckled and non-buckled locations (RMSE = 0.33, N = 61).

RMSE = 0.33, Fig. 7C). These data suggest regions with greater than ~19% fill of aggrecan are sufficiently reinforced to resist buckling.

4. Discussion

The goal of this study was to identify a relationship between local biochemical content and local mechanical properties of human tissue engineered cartilage constructs. In this study, aggrecan had the largest effect on the local shear modulus. Similarly, increasing aggrecan caused a sharp decrease in the buckling probability, and revealed a minimum local aggrecan threshold required to prevent buckling. These findings could be used to estimate and predict local mechanical function based on the local biochemical composition.

If new matrix deposition cannot prevent buckling at physiologic strains, local tissue damage and cell death may occur. Previous work has shown that chondrocyte death is correlated with high strain in native tissue (Bartell et al., 2015). Specifically, a local strain norm of greater than 18% can cause half of the chondrocytes in that region to die. Strains above 30% resulted in death of 100% of chondrocytes in that region (Bartell et al., 2015). In our engineered constructs, the high strains (E_{xx} = 15%-30%) in buckled regions could easily cause 50–100% of chondrocytes in buckled regions to die. These large strains can result in cell death under both compression or due to surface shear strains (Bartell et al., 2015; Bonnevie et al., 2016). One way to prevent local chondrocyte death and local tissue buckling is to reinforce scaffolds with new matrix deposition.

Specifically, local increases in aggrecan concentration can enhance local resistance to construct buckling. This study revealed a minimum aggrecan fraction of 0.19 is required to reduce the buckling probability. Results indicate adjacent regions of the same construct may have dramatically different abilities to resist buckling due to local aggrecan concentrations (Fig. 8). This minimum aggrecan requirement follows previous work on the relationship between global aggrecan content and the buckling probability (Middendorf et al., 2017b). Additionally, due to potentially large defects, fixing the construct may not be sufficient to prevent buckling throughout the implant. As such a minimum amount of aggrecan content is required at every location in a construct to prevent buckling, tissue damage, and to assess construct maturity prior to implantation.

The concept of a critical threshold required to prevent buckling can be explained using theory derived from tubes filled with a compliant core (Gibson et al., 2010; Karam and Gibson, 1994). The critical load that causes buckling in these tubes increases with increases in the relative density of the core to the tube (Gibson et al., 2010). If the construct behavior follows a similar theory, the scaffold can be approximated as a series of tubes stacked together. During construct growth, these tubes are filled with increasing amounts of a compliant core (i.e.: aggrecan). As such, tubes filled with a lower amount of aggrecan have a lower relative density and will be the first to buckle. Experimentally, heterogeneity in aggrecan content (Fig. 8) results in buckling probabilities between 0 and 100%. Therefore, a sigmoid curve predicted the minimum aggrecan content necessary to prevent local buckling.

In addition to theories that explain how local tissue buckling can be prevented, theories explaining the local structure function

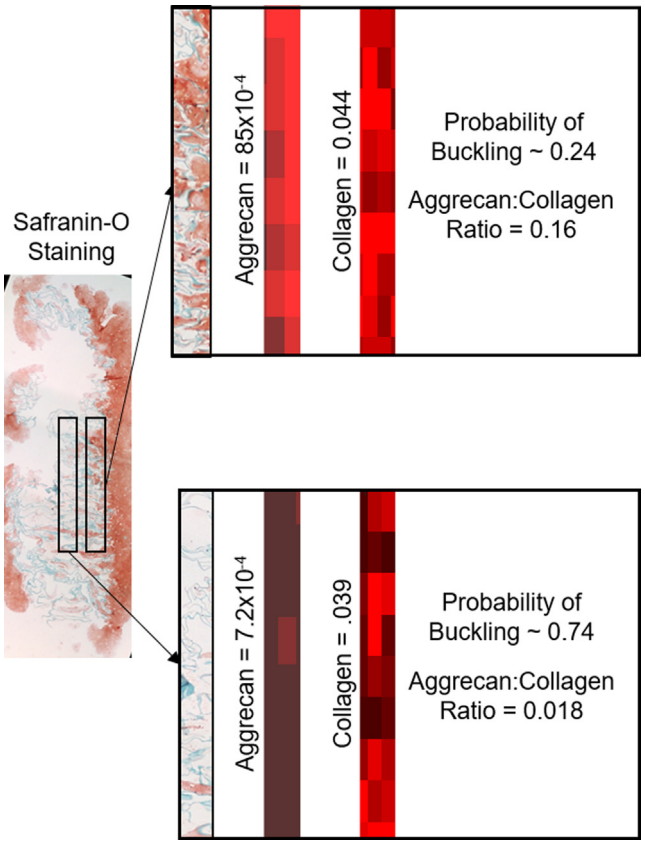

Fig. 8. Safranin-O stains and FTIR intensity images of a 5-week construct shows buckled regions have very little aggrecan filling the scaffold with similar amounts of collagen. Non-buckled regions have a large amount of aggrecan filling scaffold pores.

relationship of native articular cartilage might apply to engineered cartilage. At first glance engineered and native cartilage have two distinct structure function relationships. In engineered cartilage aggrecan not collagen was critical to improving the local shear modulus. This finding is consistent with other collagen-based constructs (Griffin et al., 2016). In contrast to native cartilage, small changes in collagen can have a large effect on the shear modulus (Silverberg et al., 2014; Stading and Langer, 1999). Still, these two distinct relationships may both be explained by one model, (i.e.: a percolation theory) (Silverberg et al., 2014), but fall on 2 distinct parts of the curve. Since the initial aggrecan content of engineered tissue is substantially different than native cartilage, theories on the local structure function relationship must be extended to encompass both native and engineered tissues.

The local structure function relationship of engineered cartilage revealed not all new matrix deposition will enhance the local tissue modulus. New matrix in the periphery region does not increase the local shear moduli or the construct's resistance to buckling. Many studies, including the current one, show preferential matrix deposition on the construct periphery (Albro et al., 2018; Kafienah et al., 2002; Klein et al., 2007; Meretoja et al., 2013; Middendorf et al., 2017a; Ng et al., 2007; Wan et al., 2011). Techniques to control the location of new matrix deposition (Cigan et al., 2016; Nims et al., 2015), including the use of physical barriers that force cells to deposit matrix inside the scaffold (Nims et al., 2017) will enhance the local shear modulus and resistance to buckling. Matrix deposition on the scaffold periphery is not ideal. The most mechanically efficient approach to improve local mechanics is to deposit matrix uniformly in the scaffold pores not on the construct periphery.

Accumulation of cells and matrix on the periphery of a construct is a feature of many scaffold systems (PGA, agarose, collagen, etc.) (Albro et al., 2018; Gooch et al., 2002; Kafienah et al., 2002; Morita et al., 2006; Ng et al., 2007) but not others (alginate) (Masuda et al., 2003; Ph et al., 2003). In order to deposit matrix uniformly throughout the scaffold pores, it may be necessary to first understand why matrix is being deposited non-uniformly in engineered cartilage constructs. In our engineered constructs, previous images have shown chondrocytes are located in both the periphery and interior regions (Middendorf et al., 2017a). This cellular distribution can be heterogeneous, therefore chondrocyte concentration might be a reason matrix is highly concentrated on the construct periphery. Multiple studies believe that lack of nutrients in the center of the construct could contribute to the reduced concentration of new matrix deposition in the interior region (Cigan et al., 2016; Kim et al., 2017; Nims et al., 2015, 2014) However, the human engineered constructs in this study typically exhibit a thinner, but just as dense periphery region on the lower surface which is always in contact with a solid plate during culture. Finally, the local cellular environment may cause some chondrocytes to produce a different concentration of new matrix compared to other chondrocytes (Ofek and Athanasiou, 2007; Taylor et al., 2018). As such, chondrocytes on the periphery may experience a different mechanical environment due to the initial collagen seeded gel and variability in the scaffold pore structure. These initial scaffold properties might be a reason new matrix deposition is contained on the scaffold periphery (Mouw et al., 2005; Wan et al., 2011). To ensure every depth of the construct has the minimum aggrecan concentration necessary to prevent buckling some of these theories may need to be investigated in more detail.

There are several challenges associated with some of the techniques used in this study. First, FTIR spectra for various types of collagen (e.g. Col I, Col II) are similar (Belbachir et al., 2009), therefore, this study could not identify the difference between the collagen scaffold (Col I) and new collagen deposition (likely Col II). Similarly, new matrix deposition that does not include collagen or aggrecan may be present. However, we determined that the lin-

ear combination technique accurately fits the raw spectra for each data point with an average coefficient of variance of 6.3% ± 3.2%. Notably, the addition of other biochemical components (including type II collagen and hyaluronan) did not significantly improve the fit and were deemed unnecessary. Additionally, we note the global mechanical (shear modulus 0.18 ± 0.12 MPa) and biochemical properties (sGAG concentration, 127 ± 9.6 μg/construct) of these constructs remained an order of magnitude less than native articular cartilage. However, previous work using this same process with a different source of human chondrocytes has shown constructs can reach similar global mechanical and biochemical properties to that of native tissue (Middendorf et al., 2017a). Finally, sectioning artifacts may decrease the accuracy of the FTIR and histology measurements taken. Multiple samples were tested to reduce the effects of sectioning artifacts and improve the observed trends. Future work could use non-destructive spectroscopy techniques to increase accuracy and the strength of these correlations. Although challenges with this study design exist, the results of this study still provide a framework to understand the effects of new matrix deposition on the local mechanics of human tissue engineered cartilage.

Depositing aggrecan content in the scaffold pores is the most efficient and effective way of improving the local shear modulus and reducing the buckling probability. The quantification of local biochemical composition is necessary to fully understand and characterize these local implant mechanics. In this study, the constructs examined were similar to those in advanced clinical trials. The relationships identified here lay the foundation necessary for future work to predict local implant mechanics using nondestructive spectroscopy techniques including Raman and IR reflectance (Albro et al., 2018; Bergholt et al., 2017, 2016; Hanifi et al., 2017; Kunstar et al., 2013). This local characterization begins to identify the minimum requirements to protect the constructs from local tissue damage and to predict the success of human tissue engineered cartilage.

Author's contributions statement

All Authors Contributed extensively to the work presented in this paper. J.M. – local biochemical and mechanical data collection and analysis and wrote manuscript; C.D, S. K. and E. C, – scaffold construct development, and results discussion; I.C. discussed the results and implications and commented on the manuscript. L.B. supervised all studies of mechanical evaluation, participated in planning of all experiments, interpretation of data, and writing and editing of the manuscript.

Acknowledgments

J.M. was funded by Cornell University and NSF GRFP grant number DGE-1650441. This research is partially funded through NSF (DMR- 1719875) and Histogenics. This work was also supported by the Advanced Regenerative Manufacturing Institute (ARMI) through the Department of Defense (grant T0080).

Conflicts of Interest

C.D. E.B. and S.K, were full time employees and stock holders of Histogenics Corp when this study was conducted. L.B is a consultant for Histogenics Corp. This research is partially funded through Histogenics.

Appendix A:. Methods

Construct preparation

Human cartilage from the femoral condyle of 2 cadavers was obtained (NDRI, Philadelphia, PA), then processed to yield chondrocytes. Constructs used a 6 mm diameter by 1.5 mm thick type I collagen honeycomb scaffold (Koken Co, Tokyo, JP). 0-week constructs were infused with an acellular collagen gel (PureCol, Advanced Biomatrix, San Diego, CA) then incubated for 24 hrs in growth media (DMEM/ F12 with 10% FBS and 1% ITS, Gibco, Thermo Fisher Scientific, Waltham, MA). Constructs at 1- and 5-weeks were seeded with a 3 mg/ml collagen gel containing chondrocytes at a concentration of $5x10^6$ cells/ml, then incubated under low oxygen conditions (2%) at 37 °C and 5% CO_2 in static culture with media changes (see above) at regular intervals.

Fourier Transform Infrared Spectroscopy (FTIR)

First, samples were fixed in 10% formalin for 24 to 48 h followed by embedding in paraffin wax. A 4 μm thick section was cut from each sample and placed on a 2 mm thick by 25 mm diameter mid-infrared (IR) transparent BaF_2 disk (Spectral Systems, Hopewell Junction, NY). Sections were dewaxed in three xylene baths, then rehydrated in three baths of ethyl alcohol (100, 95, 70% ethanol) for 2 min each.

Sections were loaded onto a Hyperion 2000 Fourier Transform infrared imaging microscope (Bruker, Billerica, MA) in transmission mode. A 15x objective was used with a slit aperture configured to acquire data on wavenumbers between 600 and 4000 cm^{-1} with an area of 79 × 160 μm. Sixteen background corrected spectra were taken and averaged to generate a single IR spectrum at each grid point. Spectra spanned the entirety of each sample such that the grid points were separated by 79 μm by 160 μm in the × and y direction, respectively.

FTIR spectra were analyzed using a previously described technique (DiDomenico et al., 2019; Rieppo et al., 2012; Silverberg et al., 2014; Yin and Xia, 2010). Each spectrum was fit to a linear combination of collagen, aggrecan, and a linear baseline from 900 to 1725 cm^{-1}. This technique has four fitting coefficients for collagen, aggrecan, and two baseline coefficients. According to Beer's law, the fitting coefficients are proportional to molecular concentration. The baseline coefficients account for instrument drift and variability that can occur during sectioning. Tissue engineered cartilage may contain other components, which are not included in this fit, however, these components are believed to produce negligible IR signatures as evidenced by a low coefficient of variation for spectral fits (6.3% ± 3.2%).

Appendix B. Supplementary material

Supplementary data to this article can be found online at https://doi.org/10.1016/j.jbiomech.2020.109760.

References

Albro, M.B., Bergholt, M.S., St-Pierre, J.P., Vinals Guitart, A., Zlotnick, H.M., Evita, E.G., Stevens, M.M., 2018. Raman spectroscopic imaging for quantification of depth-dependent and local heterogeneities in native and engineered cartilage. Regen. Med. 3, 1–10. https://doi.org/10.1038/s41536-018-0042-7.

Bartell, L.R., Fortier, L.A., Bonassar, Cohen, L.J.I., 2015. Measuring microscale strain fields in articular cartilage during rapid impact reveals thresholds for chondrocyte death and a protective role for the superficial layer. J. Biomech. 48, 3440–3446. https://doi.org/10.1016/j.jbiomech.2015.05.035.

Behrens, P., Bitter, T., Kurz, B., Russlies, M., 2006. Matrix-associated autologous chondrocyte transplantation/implantation (MACT/MACI)-5-year follow-up. Knee 13, 194–202. https://doi.org/10.1016/j.knee.2006.02.012.

Belbachir, K., Noreen, R., Gouspillou, G., Petibois, C., 2009. Collagen types analysis and differentiation by FTIR spectroscopy. Anal. Bioanal. Chem. 395, 829–837. https://doi.org/10.1007/s00216-009-3019-y.

Bergholt, M.S., Albro, M.B., Stevens, M.M., 2017. Online quantitative monitoring of live cell engineered cartilage growth using diffuse fiber-optic Raman spectroscopy. Biomaterials 140, 128–137. https://doi.org/10.1016/j.biomaterials.2017.06.015.

Bergholt, M.S., St-Pierre, J.P., Offeddu, G.S., Parmar, P.A., Albro, M.B., Puetzer, J.L., Oyen, M.L., Stevens, M.M., 2016. Raman spectroscopy reveals new insights into

the zonal organization of native and tissue-engineered articular cartilage. ACS Cent. Sci. 2, 885–895. https://doi.org/10.1021/acscentsci.6b00222.
Blaber, J., Adair, B., Antoniou, A., 2015. Ncorr: Open-source 2D digital image correlation matlab software. Exp. Mech. 55, 1105–1122. https://doi.org/10.1007/s11340-015-0009-1.
Bonnevie, E.D., Delco, M.L., Jasty, N., Bartell, L., Fortier, L.A., Cohen, I., Bonassar, L.J., 2016. Chondrocyte death and mitochondrial dysfunction are mediated by cartilage friction and shear strain. Osteoarthr. Cartil. 24, S46. https://doi.org/10.1016/j.joca.2016.01.107.
Boskey, A., Pleshko Camacho, N., 2007. FT-IR imaging of native and tissue-engineered bone and cartilage. Biomaterials 28, 2465–2478. https://doi.org/10.1016/j.biomaterials.2006.11.043.
Brittberg, M., 2010. Cell carriers as the next generation of cell therapy for cartilage repair: a review of the matrix-induced autologous chondrocyte implantation procedure. Am. J. Sports Med. 38, 1259–1271. https://doi.org/10.1177/0363546509346395.
Buckley, M.R., Bergou, A.J., Fouchard, J., Bonassar, L.J., Cohen, I., 2010. High-resolution spatial mapping of shear properties in cartilage. J. Biomech. 43, 796–800. https://doi.org/10.1016/j.jbiomech.2009.10.012.
Byers, B.A., Mauck, R.L., Change, I.E., Tuan, R.S., 2008. Transient exposure to TGF-B3 under serum-free conditions enhances the biomechanical and biochemical maturation of tissue engineered cartilage. Tissue Eng. Part A 14, 1821–1834. https://doi.org/10.1089/ten.tea.2007.0222.TRANSIENT.
Cigan, Alexander D, Durney, K.M., Nims, R.J., Vunjak-Novakovic, G., Hung, C.T., Ateshian, G.A., 2016a. Nutrient channels aid the growth of articular surface-sized engineered cartilage constructs. Tissue Eng. Part A 1 ten.TEA.2016.0179 1. https://doi.org/10.1089/ten.TEA.2016.0179.
Cigan, Alexander D., Roach, B.L., Nims, R.J., Tan, A.R., Albro, M.B., Stoker, A.M., Cook, J.L., Vunjak-Novakovic, G., Hung, C.T., Ateshian, G.A., 2016b. High seeding density of human chondrocytes in agarose produces tissue-engineered cartilage approaching native mechanical and biochemical properties. J. Biomech. 49, 1909–1917. https://doi.org/10.1016/j.jbiomech.2016.04.039.
Crawford, D.C., DeBerardino, T.M., Williams, R.J., 2012. NeoCart, an autologous cartilage tissue implant, compared with microfracture for treatment of distal femoral cartilage lesions: an FDA phase-II prospective, randomized clinical trial after two years. J. Bone Joint Surg. Am. 94, 979–989. https://doi.org/10.2106/JBJS.K.00533.
Crawford, D.C., Heveran, C.M., Cannon, W.D., Foo, L.F., Potter, H.G., 2009. An autologous cartilage tissue implant NeoCart for treatment of grade III chondral injury to the distal femur: prospective clinical safety trial at 2 years. Am. J. Sports Med. 37, 1334–1343. https://doi.org/10.1177/0363546509333011.
DiDomenico, C.D., Kaghazchi, A., Bonassar, L.J., 2019. Measurement of local diffusion and composition in degraded articular cartilage reveals the unique role of surface structure in controlling macromolecular transport. J. Biomech. 82, 38–45. https://doi.org/10.1016/j.jbiomech.2018.10.019.
Enobakhare, B.O., Bader, D.L., Lee, D.a., 1996. Quantification of sulfated glycosaminoglycans in chondrocyte/alginate cultures, by use of 1,9-dimethylmethylene blue. Anal. Biochem. 243, 189–191. https://doi.org/10.1006/abio.1996.0502.
Erickson, I.E., Huang, A.H., Chung, C., Li, R.T., Burdick, J.A., Mauck, R.L., 2009. Differential maturation and structure–function relationships in mesenchymal stem cell- and chondrocyte-seeded hydrogels. Tissue Eng. Part A 15, 1041–1052. https://doi.org/10.1089/ten.tea.2008.0099.
Freyman, T.M., Yannas, I.V., Gibson, L.J., 2001. Cellular materials as porous scaffolds for tissue engineering. Prog. Mater Sci. 46, 273–282.
Gibson, L.J., 2005. Biomechanics of cellular solids. J. Biomech. 38, 377–399. https://doi.org/10.1016/j.jbiomech.2004.09.027.
Gibson, L.J., Ashby, M.F., 1997. Cellular Solids: Structure and Properties. Cambridge University Press, Cambridge, UK.
Gibson, L.J., Ashby, M.F., Harley, B.A., 2010. Cellular Materials in Nature and Medicine. Cambridge University Press, Cambridge, UK.
Gooch, K.J., Blunk, T., Courter, D.L., Sieminski, A.L., Vunjak-Novakovic, G., Freed, L.E., 2002. Bone morphogenetic proteins-2, -12, and -13 modulate in vitro development of engineered cartilage. Tissue Eng. 8, 591–601. https://doi.org/10.1089/107632702760240517.
Griffin, D.J., Ortved, K.F., Nixon, A.J., Bonassar, L.J., 2016. Mechanical properties and structure-function relationships in articular cartilage repaired using IGF-I gene-enhanced chondrocytes. J. Orthop. Res. 34, 149–153. https://doi.org/10.1002/jor.23038.
Hanifi, A., Palukuru, U., McGoverin, C., Shockley, M., Frank, E., Grodzinsky, A., Spencer, R.G., Pleshko, N., 2017. Near infrared spectroscopic assessment of developing engineered tissues: correlations with compositional and mechanical properties. Analyst 142, 1320–1332. https://doi.org/10.1039/C6AN02167K.
Harley, B.A., Leung, J.H., Silva, E.C.C.M., Gibson, L.J., 2007. Mechanical characterization of collagen-glycosaminoglycan scaffolds. Acta Biomater. 3, 463–474. https://doi.org/10.1016/j.actbio.2006.12.009.
Kafienah, W., Jakob, M., Démarteau, O., Frazer, A., Barker, M.D., Martin, I., Hollander, A.P., 2002. Three-dimensional tissue engineering of hyaline cartilage: comparison of adult nasal and articular chondrocytes. Tissue Eng. 8, 817–826. https://doi.org/10.1089/10763270260424178.
Karam, G.N., Gibson, L.J., 1994. Biomimicking of animal quills and plant stems: natural cylindrical shells with foam cores. Mater. Sci. Eng., C 2, 113–132. https://doi.org/10.1016/0928-4931(94)90039-6.
Karchner, J.P., Yousefi, F., Darvish, K., Pleshko, N., 2017. Non-destructive spectroscopic assessment of articular cartilage correlates with mechanical properties. J. Orthop. Res. 35. https://doi.org/10.1177/1947603518764269.
Khoshgoftar, M., Wilson, W., Ito, K., Van Donkelaar, C.C., 2013. The effect of tissue-engineered cartilage biomechanical and biochemical properties on its post-implantation mechanical behavior. Biomech. Model. Mechanobiol. 12, 43–54. https://doi.org/10.1007/s10237-012-0380-0.
Kim, M., Bi, X., Horton, W.E., Spencer, R.G., Camacho, N.P., 2005. Fourier transform infrared imaging spectroscopic analysis of tissue engineered cartilage: histologic and biochemical correlations. J. Biomed. Opt. 10,. https://doi.org/10.1117/1.1922329 031105.
Kim, M., Farrell, M.J., Steinberg, D.R., Burdick, J.A., Mauck, R.L., 2017. Enhanced nutrient transport improves the depth-dependent properties of tri-layered engineered cartilage constructs with zonal co-culture of chondrocytes and MSCs. Acta Biomater. 58, 1–11. https://doi.org/10.1016/j.actbio.2017.06.025.
Klein, T.J., Chaudhry, M., Bae, W.C., Sah, R.L., 2007. Depth-dependent biomechanical and biochemical properties of fetal, newborn, and tissue-engineered articular cartilage. J. Biomech. 40, 182–190. https://doi.org/10.1016/j.jbiomech.2005.11.002.
Kon, E., Filardo, G., Di Matteo, B., Perdisa, F., Marcacci, M., 2013. Matrix assisted autologous chondrocyte transplantation for cartilage treatment: a systematic review. Bone Joint Res. 2, 18–25. https://doi.org/10.1302/2046-3758.22.2000092.
Krase, A., Abedian, R., Steck, E., Hurschler, C., Richter, W., 2014. BMP activation and Wnt-signalling affect biochemistry and functional biomechanical properties of cartilage tissue engineering constructs. Osteoarthr. Cartil. 22, 284–292. https://doi.org/10.1016/j.joca.2013.11.011.
Kunstar, A., Leferink, A.M., Okagbare, P.I., Morris, M.D., Roessler, B.J., Otto, C., Karperien, M., van Blitterswijk, C.A., Moroni, L., van Apeldoorn, A.A., 2013. Label-free Raman monitoring of extracellular matrix formation in three-dimensional polymeric scaffolds. J. R. Soc. Interface 10, 20130464. https://doi.org/10.1098/rsif.2013.0464.
Leroux, M.A., Arokoski, J., Vail, T.P., Guilak, D., Hyttinen, M.M., Kiviranta, I., Setton, L. A., 2000. Simultaneous Changes in the Mechanical Properties, Quantitative Collagen Organization, and Proteoglycan Concentration of Articular Cartilage following. Canine Meniscectomy.
Luo, L., Chu, J.Y.J., Eswaramoorthy, R., Mulhall, K.J., Kelly, D.J., 2017. Engineering tissues that mimic the zonal nature of articular cartilage using decellularized cartilage explants seeded with adult stem cells. ACS Biomater. Sci. Eng. 3, 1933–1943. https://doi.org/10.1021/acsbiomaterials.6b00020.
Masuda, K., Sah, R.L., Hejna, M.J., Thonar, E.J.M.A., 2003. A novel two-step method for the formation of tissue-engineered cartilage by mature bovine chondrocytes: the alginate-recovered-chondrocyte (ARC) method. J. Orthop. Res. 21, 139–148. https://doi.org/10.1016/S0736-0266(02)00109-2.
Mauck, R.L., Seyhan, S.L., Ateshian, G.A., Hung, C.T., 2002. Influence of seeding density and dynamic deformational loading on the developing structure/function relationships of chondrocyte-seeded agarose hydrogels. Ann. Biomed. Eng. 30, 1046–1056. https://doi.org/10.1114/1.1512676.
Meretoja, V.V., Dahlin, R.L., Wright, S., Kasper, F.K., Mikos, A.G., 2013. The effect of hypoxia on the chondrogenic differentiation of co-cultured articular chondrocytes and mesenchymal stem cells in scaffolds. Biomaterials 34, 4266–4273. https://doi.org/10.1016/j.biomaterials.2013.02.064.
Middendorf, J.M., Griffin, D.J., Shortkroff, S., Dugopolski, C., Kennedy, S., Siemiatkoski, J., Cohen, I., Bonassar, L.J., 2017a. Mechanical properties and structure-function relationships of human chondrocyte-seeded cartilage constructs after in vitro culture. J. Orthop. Res. 1–9. https://doi.org/10.1002/jor.23535.
Middendorf, J.M., Shortkroff, S., Dugopolski, C., Kennedy, S., Siemiatkoski, J., Bartell, L.R., Cohen, I., Bonassar, L.J., 2017b. In vitro culture increases mechanical stability of human tissue engineered cartilage constructs by prevention of microscale scaffold buckling. J. Biomech. 64, 77–84. https://doi.org/10.1016/j.jbiomech.2017.09.007.
Morita, Y., Tomita, N., Aoki, H., Sonobe, M., Wakitani, S., Tamada, Y., Suguro, T., Ikeuchi, K., 2006. Frictional properties of regenerated cartilage in vitro. J. Biomech. 39, 103–109. https://doi.org/10.1016/j.jbiomech.2004.10.031.
Mouw, J.K., Case, N.D., Guldberg, R.E., Plaas, A.H.K., Levenston, M.E., 2005. Variations in matrix composition and GAG fine structure among scaffolds for cartilage tissue engineering. Osteoarthr. Cartil. 13, 828–836. https://doi.org/10.1016/j.joca.2005.04.020.
Neuman, R.E., Logan, M.A., 1950. The determination of Hydroxyproline. J. Biol. Chem., 299–306
Ng, K.W., Saliman, J.D., Lin, E.Y., Statman, L.Y., Kugler, L.E., Lo, S.B., Ateshian, G.A., Hung, C.T., 2007. Culture duration modulates collagen hydrolysate-induced tissue remodeling in chondrocyte-seeded agarose hydrogels. Ann. Biomed. Eng. 35, 1914–1923. https://doi.org/10.1007/s10439-007-9373-z.
Ng, K.W., Wang, C.C.B., Mauck, R.L., Kelly, T.A.N., Chahine, N.O., Costa, K.D., Ateshian, G.A., Hung, C.T., 2005. A layered agarose approach to fabricate depth-dependent inhomogeneity in chondrocyte-seeded constructs. J. Orthop. Res. 23, 134–141. https://doi.org/10.1016/j.orthres.2004.05.015.
Nims, R.J., Cigan, A.D., Albro, M.B., Hung, C.T., Ateshian, G.A., 2014. Synthesis rates and binding kinetics of matrix products in engineered cartilage constructs using chondrocyte-seeded agarose gels. J. Biomech. 47, 2165–2172. https://doi.org/10.1016/j.jbiomech.2013.10.044.
Nims, R.J., Cigan, A.D., Albro, M.B., Vunjak-novakovic, G., Hung, C.T., Ateshian, G.A., 2015. Matrix production in large engineered cartilage constructs is enhanced by nutrient channels and excess media supply. Tissue Eng. Part C 21, 747–757. https://doi.org/10.1089/ten.tec.2014.0451.
Nims, R.J., Cigan, A.D., Durney, K.M., Jones, B.K., O'Neill, J.D., Law, W.-S.A., Vunjak-Novakovic, G., Hung, C.T., Ateshian, G.A., 2017. Constrained cage culture

improves engineered cartilage functional properties by enhancing collagen network stability. Tissue Eng. Part A 23, 847–858. https://doi.org/10.1089/ten.tea.2016.0467.

Nixon, A.J., Rickey, E., Butler, T.J., Scimeca, M.S., Moran, N., Matthews, G.L., 2015. A chondrocyte infiltrated collagen type I/III membrane (MACI® implant) improves cartilage healing in the equine patellofemoral joint model. Osteoarthr. Cartil. 23, 648–660. https://doi.org/10.1016/j.joca.2014.12.021.

Ofek, G., Athanasiou, K.A., 2007. Micromechanical properties of chondrocytes and chondrons: relevance to articular cartilage tissue engineering. J. Mech. Mater. Struct. 2, 1059–1086. https://doi.org/10.2140/jomms.2007.2.1059.

Ph, D., Masuda, K.M.D., D, E.J.A.T.P., Sah, R.L.M.D., Sc, D., 2003. Tissue engineering of stratified articular cartilage from chondrocyte subpopulations 4584, 595–602. 10.1016/S1063-4584(03)00090-6.

Poole, A.R., Kojima, T., Yasuda, T., Mwale, F., Kobayashi, M., Laverty, S., 2001a. Composition and structure of articular cartilage: a template for tissue repair. Clin. Orthop. Relat. Res. 1. S26–S33. 11603710.

Poole, R., Kojima, T., Kobayashi, M., 2001b. Composition and Structure of Articular Cartilage.

Puetzer, J.L., Brown, B., Ballyns, J., Bonassar, L.J., 2013. The effect of IGF-I on anatomically shaped tissue-engineered menisci. Tissue Eng. Part A 19, 1443–1450. https://doi.org/10.1089/ten.tea.2012.0645.

Rieppo, L., Rieppo, J., Jurvelin, J.S., Saarakkala, S., 2012. Fourier transform infrared spectroscopic imaging and multivariate regression for prediction of proteoglycan content of articular cartilage. PLoS ONE 7. https://doi.org/10.1371/journal.pone.0032344.

Rosenberg, L., 1971. Chemical basis for the histological use of safranin O in the study of articular cartilage. J. Bone Joint Surg. Am. 53, 69–82.

Schinagl, R.M., Gurskis, D., Chen, a.C., Sah, R.L., 1997. Depth-dependent confined compression modulus of full-thickness bovine articular cartilage. J. Orthop. Res. 15, 499–506. https://doi.org/10.1002/jor.1100150404.

Silverberg, J.L., Barrett, A.R., Das, M., Petersen, P.B., Bonassar, L.J., Cohen, I., 2014. Structure-function relations and rigidity percolation in the shear properties of articular cartilage. Biophys. J. 107, 1721–1730. https://doi.org/10.1016/j.bpj.2014.08.011.

Silverberg, J.L., Dillavou, S., Bonassar, L., Cohen, I., 2013. Anatomic variation of depth-dependent mechanical properties in neonatal bovine articular cartilage. J. Orthop. Res. 31, 686–691.

Stading, M., Langer, R., 1999. Mechanical shear properties of cell-polymer cartilage constructs. Tisssue Eng. 5, 241–250.

Steck, E., Ph, D., Bertram, H., Ph, D., Walther, A., Ph, D., Brohm, K., Mrozik, B., Rathmann, M., Merle, C., Gelinsky, M., Ph, D., Richter, W., Ph, D., 2010. Enhanced Biochemical and Biomechanical Properties of Scaffolds Generated by Flock Technology 16. 10.1089/ten.tea.2009.0817.

Taylor, D.A., Sampaio, L.C., Ferdous, Z., Gobin, A.S., Taite, L.J., 2018. Decellularized matrices in regenerative medicine. Acta Biomater. https://doi.org/10.1016/j.actbio.2018.04.044.

Wan, L.Q., Jiang, J., Miller, D.E., Guo, X.E., Mow, V.C., Lu, H.H., 2011. Matrix deposition modulates the viscoelastic shear properties of hydrogel-based cartilage grafts. Tissue Eng. Part A 17, 1111–1122. https://doi.org/10.1089/ten.tea.2010.0379.

Williamson, A.K., Chen, A.C., Sah, R.L., 2001. Compressive properties and function – composition relationships of developing bovine articular cartilage. J. Orthop. Res. 19, 1113–1121. https://doi.org/10.1016/S0736-0266(01)00052-3.

Wilson, W., Huyghe, J.M., Van Donkelaar, C.C., 2007. Depth-dependent compressive equilibrium properties of articular cartilage explained by its composition. Biomech. Model. Mechanobiol. 6, 43–53. https://doi.org/10.1007/s10237-006-0044-z.

Wu, J.Z., Herzog, W., 2002. Elastic anisotropy of articular cartilage is associated with the microstructures of collagen fibers and chondrocytes. J. Biomech. 35, 931–942.

Yin, J., Xia, Y., 2010. Macromolecular concentrations in bovine nasal cartilage by Fourier transform infrared imaging and principal component regression. Appl. Spectrosc. 64, 1199–1208.